Robust self-cleaning and marine anticorrosion super-hydrophobic Co-Ni/CeO_2 composite coating

Yanpeng Xue[a,=,*], Shuqiang Wang[a,=], Yanyan Xue[b], Lili Cao[c], Mengyan Nie[d], Ying Jin[a*]

[a]National Center for Materials Service Safety, University of Science and Technology Beijing, Xueyuan Road 30, 100083, Beijing, China
[b]School of Physics Science and Engineering, Institute for Advanced Study, Tongji University, Shanghai, 200092, China
[c]School of Mechanical and Energy Engineering, Zhejiang University of Science and Technology, Liuhe Road 318, Hangzhou, China
[d]Institute for Materials Discovery, University College London, Malet Place, London, WC1E 7JE, UK.

=These authors contributed equally to this work
* Corresponding Author: yanpengxue@ustb.edu.cn; yjin@ustb.edu.cn.

Abstract:

Until now, super-hydrophobic materials that are scale-up fabrication and application to harsh environments remain challenging because of their fragile mechanical durability. Because of their unique electronic structure, Rare-earth oxides (REOs) have been proven to be intrinsically hydrophobic. Herein, cerium oxide particles (CeO_2) are added to the coating by co-electrodeposition. The Co-Ni/CeO_2 composite coating from the electrolyte containing 3.44 g/L possesses a flower-like hierarchical structures, displaying a super-hydrophobic behavior after the modification by PFTEOS. More importantly, excellent mechanical durability with critical abrasion distance of 22.5 m is achieved under a 5 kPa fixed normal pressure in the liner abrasion test before the loss of super-hydrophobicity. And electrochemical measurements demonstrate that the super-hydrophobic composite coatings display high corrosion resistance.

1. Introduction

Biomimetic surfaces with super-hydrophobicity have been extensively explored for applications in corrosion protection[1,2], water/oil separation[3,4], anti-icing[5], self-cleaning[6,7] and drag reduction[8]. In general, these surfaces exhibit the wetting characteristic of a water contact angle (WCA) above 150° and a water sliding angle (WSA) below 10°[9]. The super-hydrophobic surfaces

This article has been accepted for publication and undergone full peer review but has not been through the copyediting, typesetting, pagination and proofreading process, which may lead to differences between this version and the Version of Record. Please cite this article as doi: 10.1002/adem.202000402.

achieve distinct non-wetting properties through the combination of chemical compositions and hierarchical structures. Many techniques, such as chemical or electrochemical etching[10], chemical vapor deposition[11], laser processing[12,13], colloidal synthesis[14,15] and anodic oxidation[16] have been exploited for fabrication of effective artificial super-hydrophobic surfaces. However, all these methods involve complex treatments and/or expensive materials, limiting their mass production. In addition, poor mechanical durability of as-fabricated micro-nano structures further restrains their commercialization process[17,18].

The microstructures of the surface are of vital importance for achieving super-hydrophobicity and improving wear resistance[9,19]. For example, the elongated branch-like structures[20] are more susceptible to mechanical damage than the cauliflower-like structures[21]. It is also well known that dispersion of second phase fine ceramic particles can effectively enhance the mechanical properties. He et al. fabricated eco-friendly and mechanical durable superhydrophobic surface from the suspension of eggshell and ZnO particles, which could keep superhydrophobicity after 3.6 m abrasion length of 600 # sandpaper under the load of 100 g[22]. As a well-established technique, electrochemical deposition has been proven to enable controlling hierarchical structures and surface morphologies of the coatings deposited onto conductive substrates for improving wear and corrosion resistance[23,24]. As a result, electrochemical deposition can be considered as a simple, scalable and low-cost technique for effective fabrication of large-area metallic super-hydrophobic coatings with high wear-resistance. For example, the nickel-based super-hydrophobic coatings on magnesium alloy modified by stearic acid only maintain its hydrophobicity in a length of 0.7 m under 1.2 kPa abrasive pressure[25], while electrodeposited Ni/PTFE composite coatings maintained super-hydrophobicity for significantly longer abrasion lengths, e.g. a length of 50 m under 2 kPa applied abrasion pressure[26]. Zhao et al. demonstrated wear resistance of the electrodeposited Ni-WS_2 coating cab be significantly improved by adding WS_2 particles while its super-hydrophobicity was preserved within an abrasion length of 1.25 m under a higher applied abrasion pressure of 2.83 kPa[27]. By electrochemical co-deposition of hardened WC and lubricated WS_2 nanosized particles, a more robust super-hydrophobic coating was achieved with 10 m abrasion length under the applied pressure of 3.0 kPa[28].

However, Rare-earth oxides (REOs) as a second phase particles received less attention on the fabrication of super-hydrophobic coatings. Azimi et al. demonstrated the intrinsically hydrophobic properties of REOs due to their unique electronic structures[29]. Through sputtering ceria onto silicon microposts, they fabricated super-hydrophobic surfaces. However, the super-hydrophobic properties were easily destroyed because of the fragile silicon textures when subjected to abrasive wear[29]. Later, Tam et al. electrodeposited Ni/CeO_2 composite coatings, which displayed remarkable non-wetting properties with water contact angle of 132° maintained even after 720 m of abrasive wear under 4 kPa applied pressure[30].

In our previous work, super-hydrophobic Co-Ni coatings with excellent wear resistance have been prepared via electrochemical deposition [21]. In this work, a new class of Co-Ni/CeO_2 composite coatings were obtained from the mixed solution by adding the as-received CeO_2 particles. After modification with low energy material, the Co-Ni/CeO_2 composite coating exhibits high WCA (160.7°), ultralow WSA (2°) and self-cleaning effect. More interesting, the linear abrasion test confirmed that the as-prepared composite coating could maintain the critical abrasion distance of 22.5

m before the loss of super-hydrophobicity. Furthermore, compared to the carbon steel substrate, the corrosion current density dropped 2 orders of magnitude for the as-prepared super-hydrophobic coatings.

2. Experimental Section

2.1 Sample preparation. The electrodeposition process has been introduced elsewhere using three electrode system with saturated calomel electrode (SCE) as the reference electrode [21]. The commercial carbon steel (20#) is cut into the size of 10 mm × 10 mm × 3 mm and used as substrate. The carbon steel substrate is sealed in epoxy and used as the working cathode. Before electrodeposition, the samples are polished by SiC sandpapers. Afterwards, the samples are electrodeposited at -65 mA/cm^2 for 2000 s.

For the electrodeposition of Co-Ni/CeO_2 coatings, the solution of 0.1 mol L^{-1} $CoCl_2 \cdot 6H_2O$, 0.03 mol L^{-1} $NiCl_2 \cdot 6H_2O$, 0.1 mol L^{-1} H_3BO_3 (Sino pharm Chemical Reagent) and different amounts of CeO_2 particles (99.9%, Aladdin) was used. To achieve homogeneous distribution of CeO_2 particles among the coating, the solution was kept stirring with a magnetic stirrer at approximately 800 rpm.

After electrodeposition, the samples were immersed into the ethanol solution of 20 mL 5 wt.% 1H,1H,2H,2H-Perfluorooctyltrichlorosilane ($C_{48}H_4Cl_3F_{13}Si$, PFTEOS, Beijing Bailingwei Technology Company) for 1 h. Then the samples were washed for investigation.

2.2 Characterization of the coatings. The surface topographies and elemental contents of the as-prepared samples were observed through SEM (EVO MA 25/LS 25) and EDS, (Oxford Instruments). The water contact angles (WCA) and water sliding angles (WSA) of the samples were measured by the automatic goniometer (Model SCA20, Kino industries ltd) with water volumes of around 5 μL and 12 μL, respectively. The crystal structures of the as-deposited samples were obtained by XRD (Rigaku Smart Lab 9 KW). The chemical states of the elements on the samples top surface were investigated with XPS (Kratos Axis Ultra DLD). The self-cleaning effect was tested using a dust of white Al_2O_3 particles and distilled water. The images of the self-cleaning properties were captured by a digital camera (Canon EOS 6D).

2.3 Linear abrasion test. To assess the wear resistance of the prepared super-hydrophobic coating, linear abrasion test was conducted on a scratch tester with 800# SiC abrasive paper. The samples were pulled against the abrasive paper with different distances at a rate of 5 mm/s under an applied pressure of 5 kPa. During the linear abrasion test, the change of contact angles were also recorded.

2.4 Corrosion resistance. Using the three-electrode conventional cell (the Pt plate as counter electrode and the saturated calomel electrode SCE as reference electrode), the electrochemical behavior of the as-prepared composite coatings as the working electrode was assessed in a 3.5 wt.% NaCl solution with a Gamry Reference 3000 Potentiostat (Gamry Instruments). Before each test, the samples were put in the testing electrolyte for 1 h. The EIS measurements were performed at open-circuit potential in a frequency range of 10^5 Hz to 0.01 Hz under the amplitude signal of 5 mV. The obtained EIS data were analyzed using the ZSimpWin (Version 3.3) software. After EIS, the polarization curves were performed between -1.3 to -0.4 mV vs SCE at a sweep speed of 0.5 mV/s.

3. Results and Discussions

The Co-Ni/CeO_2 composite coatings with hierarchical structures were successfully fabricated on bare carbon steel using the electrochemical deposition by adding CeO_2 particles in the electrolyte solutions. At first, the morphologies of the used CeO_2 particles were characterized. By the low magnification SEM image (Fig. 1a), the CeO_2 ceramic particles are irregular in shape with the sizes ranged from a few micrometers to a few tens micrometers. From the high magnification SEM image (Fig.1b), it is noted that the large particles are loose with the surfaces attached with a great amount of nano-sized CeO_2 particles

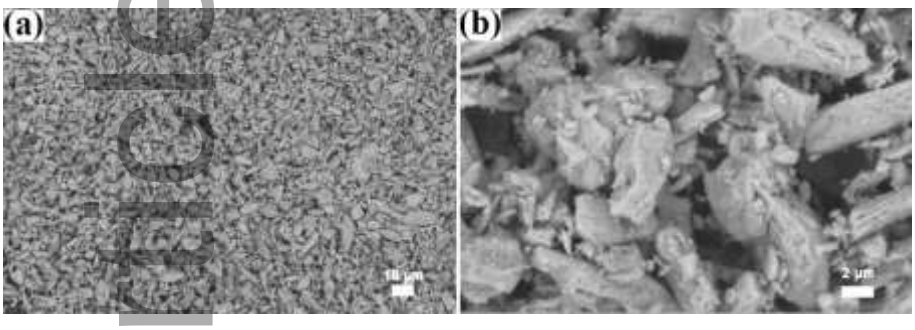

Figure 1. Surface morphology of CeO_2 particles (a) low enlargement and (b) high enlargement.

The typical surface topographies of the carbon steel substrate after polishing and the Co-Ni coating electrodeposited at -1.7 V vs. SCE in the bath solution of 0.1 mol/L $CoCl_2 \cdot 6H_2O$, 0.03 mol/L $NiCl_2 \cdot 6H_2O$ and 0.1 mol/L H_3BO_3 are shown in Fig.S1. It is clearly shown that the Co-Ni coatings with cauliflower-shaped hierarchical structures were obtained (Fig.S1b). Fig.2 illustrated the surface topography variation of Co-Ni/CeO_2 composite coatings electrodeposited at constant current density of -65 mA/cm^2 with different contents of CeO_2 particles added in the above-mentioned mixed solution. When the content of CeO_2 particles in the electrolyte solution was 1.72 g/L, irregular diamond-like structures having a diameter of about several micrometers were aggregated to form a larger-sized irregular structure, and distributed uniformly over the entire surface (Fig.2a and 2d). After doubling the CeO_2 content to 3.44 g/L, parts of the diamond structures were replaced by the flaky fish scale structures, and further aggregated into the flower-like micro/nano hierarchical structures (Fig. 2b and 2e). With the CeO_2 content rose to 6.88 g/L in the mixed solution, the flower-like micro/nano hierarchical structures were replaced by locally aggregated CeO_2 clusters, which were distributed inhomogeneously on the surface (Fig. 2c and 2f). Cross section images of the as-prepared composite coatings were provided (Figure S2 in the supporting information). According to the cross section images, the thickness of the composite coating electrodeposited in the mixed solution containing CeO_2 particles of 1.72 g/L was around 15 μm after the deposition time of 2000 s. With the increase of the CeO_2 particles to 3.44 g/L, the thickness of the electrodeposited composite coating increased to 20 μm. However, by adding the CeO_2 particles to 6.88 g/L, the electrodeposited coating's thickness decreased to 16 μm, which could be attributed to the difficulty of co-electrodeposition due to the large amount of CeO_2 particles.

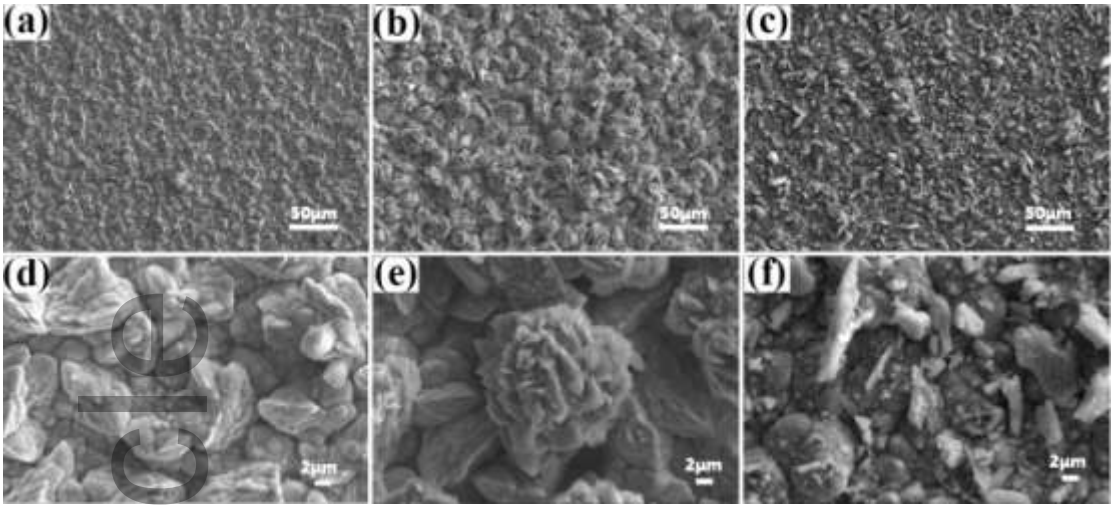

Figure 2. Surface topography of Co-Ni/CeO_2 composite coatings electrodeposited at the current density of -65 mA/cm^2 for 2000 s in the mixed solutions containing CeO_2 particles of: (a,d) 1.72 g/L; (b,e) 3.44 g/L; and (c,f) 6.88 g/L.

According to the EDS analysis shown in Table 1, the CeO_2 contents were around 12.4 wt.% (Fig.2a), 15.6 wt.% (Fig.2b) and 19.1 wt.% (Fig.2c) in the corresponding Co-Ni/CeO_2 composite coatings respectively. Under the same deposition conditions, the CeO_2 content in the coatings gradually increased while the nickel in the composite deposits content decreased.

Table 1. The chemical compositions of the coatings electrodeposited at -65 mA/cm^2 for 2000 s.

	1.72 g/L	3.44 g/L	6.88 g/L
Co(wt.%)	73.4	75.8	74.1
Ni(wt.%)	13.6	6.8	4.5
Ce(wt.%)	12.4	15.6	19.1
O(wt.%)	0.6	1.8	2.3

The EDS mappings were conducted to further reveal the distribution of the CeO_2 particles within the hierarchical structures. The obtained results demonstrated that the elements cobalt and nickel covered the whole surface of the coating and different sizes of CeO_2 particles were embedded in the Co-Ni coating. As shown in Fig.3a, a small amount of CeO_2 particles were intercalated inside the coating. With the increase of CeO_2 particle content to 3.44 g/L, element cerium was mainly distributed in the hierarchical structures, which might be the reason for the formation of flower-like micro/nano hierarchical structures (Fig.3b). As the CeO_2 particles rose to 6.88 g/L in the electrolyte solution, Fig.3c showed the irregular shaped CeO_2 particles were distributed throughout the surface of the composite coating.

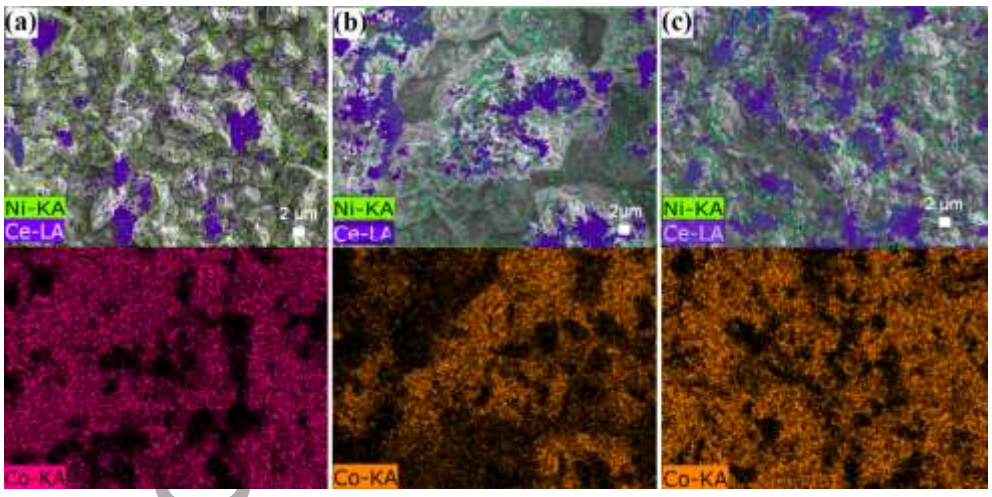

Figure 3. EDS elemental distribution mapping of the coatings electrodeposited at -65 mA/cm^2 for 2000 s with different amount of CeO_2 particles: a) 1.72 g/L; b) 3.44 g/L; c) 6.88 g/L.

The X-ray diffraction patterns of CeO_2 particles, electrodeposited Co-Ni coating and Co-Ni/CeO_2 composite coatings were displayed in Figure 4. For the CeO_2 particles, the peaks at 28.55°, 33.08°, and 47.47° could be attributed to the (111), (200), and (220) crystalline planes of fcc CeO_2 (JCPDS file no.34-0394). The pure Co-Ni coating showed three main peaks at 44.2°, 51.5° and 75.9°, which could be ascribed to fcc Co (JCPDS file no.89-7093) crystalline planes (111), (200), and (220). However, nickel peak wasn't detected, which could be ascribed to the formation of homogeneous Co-Ni solid solutions[31,32].

The diffraction patterns of the three electrodeposited Co-Ni/CeO_2 composite coatings (Fig.4c-4e) exhibited the peaks at 44.2°, 51.5° and 75.9°, which could correspond to fcc Co crystalline planes. And the diffraction peaks near 28.55°, 33.08°, and 47.47° were assigned respectively to (111), (200), (220) crystalline planes of fcc CeO_2. The diffraction patterns of the Co-Ni/CeO_2 composite coatings indicated the existence of Co-Ni alloy and the CeO_2 particles. After incorporating different amount of micro-nano CeO_2 particles, the relative Co-Ni peaks intensities displayed minor changes, which indicated a small variation in the crystal orientation of the Co-Ni grains compared with pure Co-Ni coating.

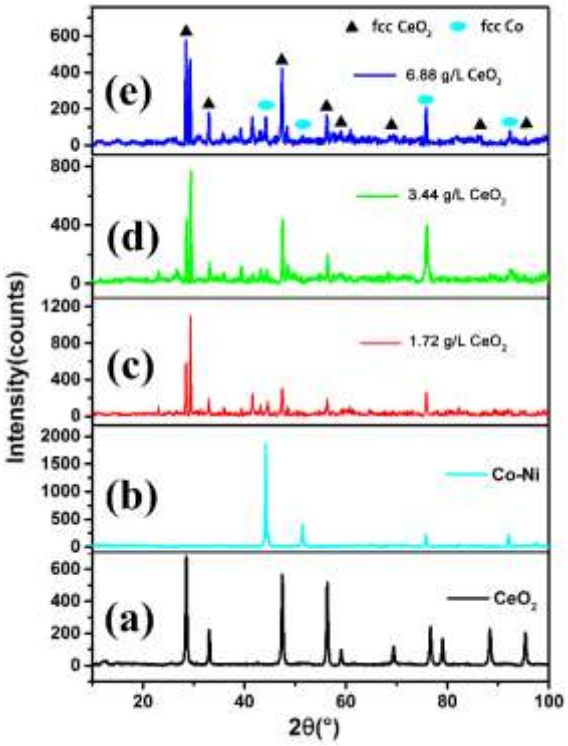

Figure 4. XRD patterns of (a) CeO_2 powders; (b) the electrodeposited Co-Ni coating and the Co-Ni/CeO_2 coatings electrodeposited with the CeO_2 particles contents of: (c) 1.72 g/L; (d) 3.44 g/L and (e) 6.88 g/L in the mixed solution.

Lots of works devoted to understand the wetting properties of solid materials over the past decades and surface polarity has been probed to govern a material's affinity towards water molecules[33,34]. Common metals tend to be hydrophilic due to lots of polar sites on their surface, and general hierarchical micro/nano structures always facilitate the super-hydrophilicity as the microstructure as a path for water circulation. In contrast, due to their unique electronic structure, rare-earth oxides (REOs) are anticipated to exhibit hydrophobic wetting properties[29]. In our previous work[21], the water contact angles of the electrodeposited Co–Ni coatings with hierarchical structures before modification were almost zero, exhibiting the super-wetting behavior. However, by adding the CeO_2 particles of 1.72 g/L and 6.88 g/L in the electroplating solution, the contact angles of the electrodeposited Co-Ni/CeO_2 composite coatings were close to 140° (Fig. 5a), which was similar to the Ni/CeO_2 composite coatings with contact angle of 132°[30]. These results demonstrated that the addition of CeO_2 particles in the electrodeposits could lead to remarkable non-wetting properties.

In order to obtain super-hydrophobicity, PFTEOS ($C_{48}H_4Cl_3F_{13}Si$) was used to decrease the surface energy and the variation of the wetting properties was displayed in Fig.5a. After modification, the self-assembled film was formed due to the reaction of PFTEOS molecules with the -OH groups on the composite coating surface, which reduce the polar sites, leading to its super-hydrophobicity [16]. As can be seen in Fig.5a, the Co-Ni/CeO_2 coating electrodeposited in the electroplating solution with the 3.44 g/L CeO_2 particles exhibits a better super-hydrophobicity (WCA=160.7°, WSA=2°), revealing that the flower-like hierarchical micro/nano structures could lead to a better super-hydrophobicity.

To further explain the conversion of the wetting properties, the X-ray photoelectron spectroscopy (XPS) was implemented on the coating surface electrodeposited with the 3.44 g/L CeO_2 particles

before and after PFTEOS modification (Fig.5b and 5c). In the full XPS survey spectrum, the C 1s (284.78 eV), O 1s (532.15 eV), Co 2p (778.1 eV), Ni 2p (852.2 eV) and Ce 3d (907.3 eV) peaks were detected for the sample before PFTEOS modification. After modification with PFTEOS, strong signal related to F element appeared on the XPS full survey spectra (Fig. 5b), and the signals of Co 2p, Ni 2p and Ce 3d core levels were reduced. As shown in Fig.5c, only three peaks assigned to C-C, C-O-C and O=C=O groups of C 1s existed on sample surface before PFTEOS modification. However, intensive F 1s peaks appeared in the XPS survey spectrum of PFTEOS modified Co-Ni/CeO_2 coating surface. And the identification $–CF_2$ group and $–CF_2$-CF_3 group could be found at 291.2 and 289.2 eV, respectively. The XPS results suggested that the low energy material molecules have successfully immobilized on the electrodeposited Co-Ni/CeO_2 coating surface and the presence of –CFx moieties efficiently reduced the surface energy.

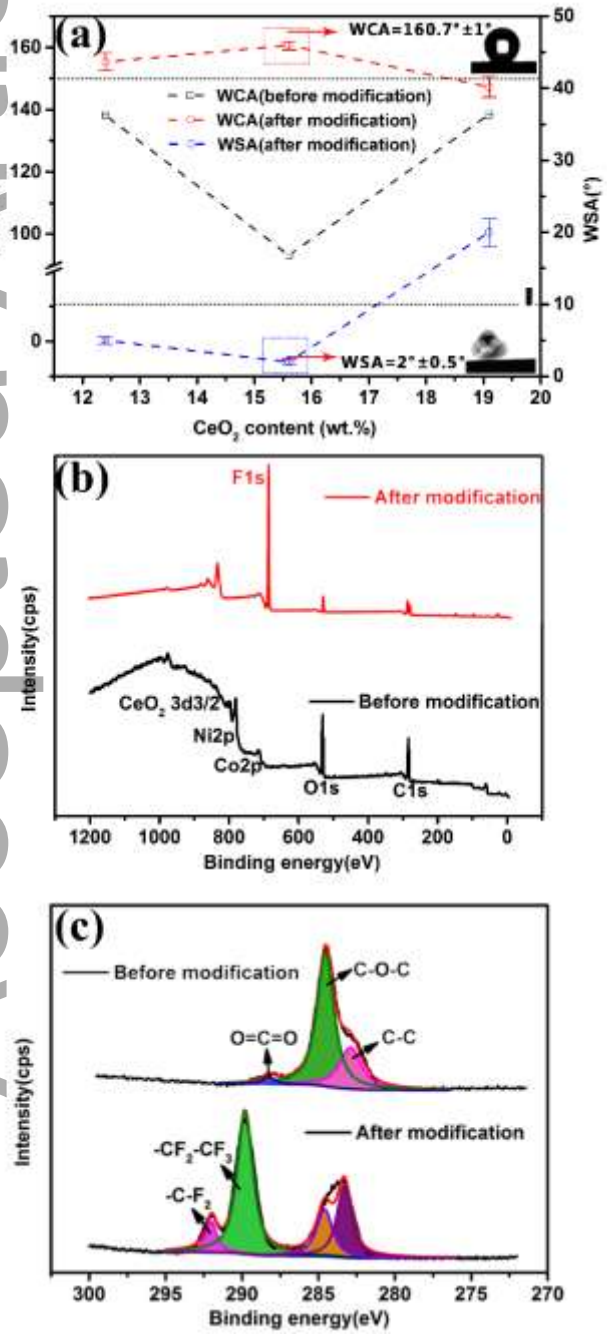

Figure 5. (a) the WCA and WSA variations with CeO_2 contents before and after modification by PFTEOS molecules; XPS spectra of the Co-Ni/CeO_2 coating electrodeposited with 3.44 g/L CeO_2 particles : (b) full XPS survey spectra and (c)

C1s XPS spectra.

In order to evaluate the mechanical durability, linear abrasion test was advised to be adopted by Ras et al. [35]. Therefore, in our study the linear abrasion test, which derived from ASTM D4060, was adopted to assess the mechanical durability of the as-prepared Co-Ni/CeO_2 coating electrodeposited with 3.44 g/L CeO_2 particles, in which the as-prepared sample was rubbed in a reciprocation motion against the 800 grit SiC abrasive paper at a speed of 5 mm/s under a 5 kPa fixed normal pressure.

Fig. 6 showed the loss of the hierarchical structures on the coating surface during the linear abrasion test, in which the super-hydrophobic property degraded gradually with the decrease in WCA and the increase in WSA. When the abrasion distance was within 1.5 m (Fig.6b), very few flaky fish scale structures were worn out due to the existence of convex structures and most hierarchical structures were preserved during the abrasion test, which explained the fact that the super-hydrophobic nature of our coating was hardly affected. Those air cushions trapped among the gaps prevented the droplets from permeation. When the abrasion distance increased to 18 m, large area flaky fish scale structures were worn out by about half but the second level structures were still preserved (Fig.6c). The preserved micro-nano structures were still capable of trapping air within the flaky fish scale structures. As a result, the WCA reduced by about 7 degrees and the WSA increased by 6 degrees. The super-hydrophobic behavior was still maintained. With the increase of the abrasion distance to 30 m, the hierarchical structures were worn out (Fig.6d). The WCA decreased to around 150° and the WSA increased to 19°, indicating the loss of super-hydrophobicity. From Fig.6e, it could be noted that WCA decreased and WSA increased linearly with the increase of the abrasion distances. Towards the loss of super-hydrophobic property, the critical abrasion distance was around 22.5 m. Meanwhile, the surface roughness was measured to characterize the surface wear loss during the linear abrasion test (Fig.6f). The surface roughness decreased linearly with the abrasion distance and the R_a value was close to 5 μm when the abrasion distance was 22.5 m. In comparison to the initial value before the linear abrasion test, the surface roughness value decreased by 5.4.

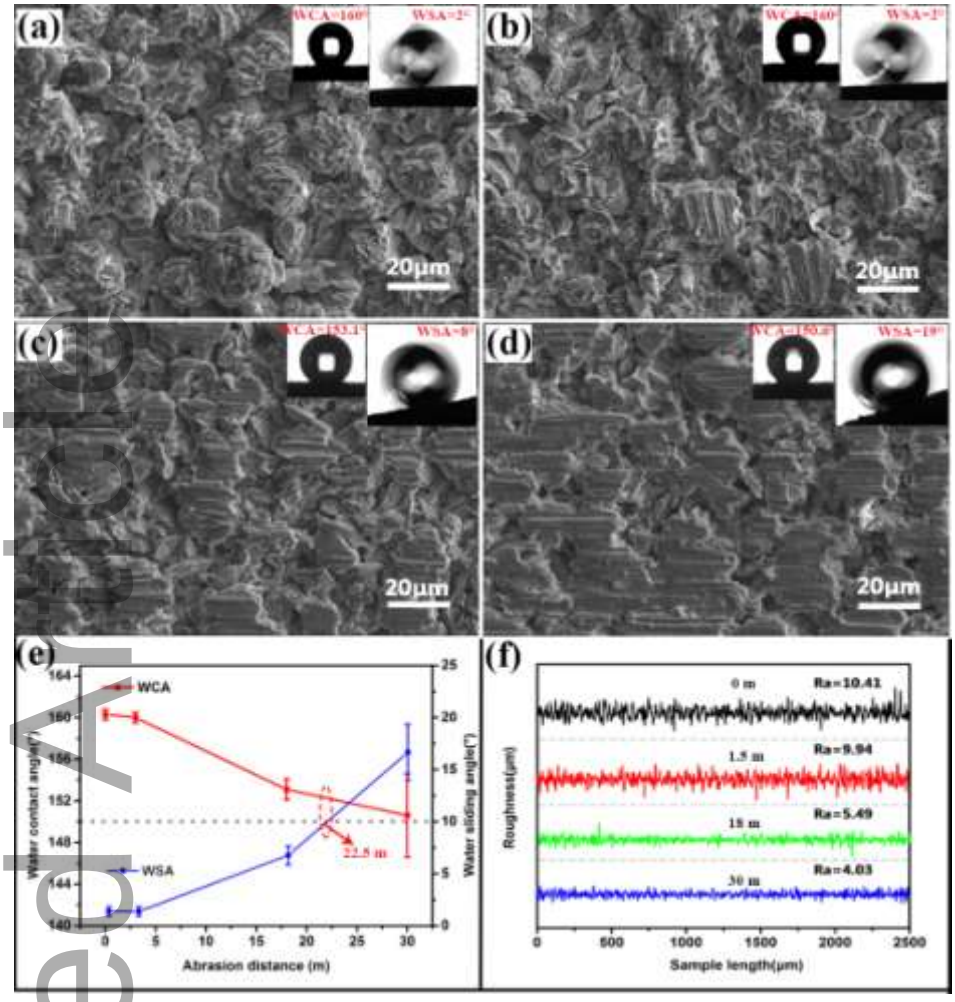

Figure 6. SEM images of the super-hydrophobic Co-Ni/CeO_2 coating electrodeposited with 3.44 g/L CeO_2 particles after different abrasion distances (a) 0 m; (b) 1.5 m; (c) 18 m and (d) 30 m. (e) WCA and WSA variations and (f) the corresponding surface roughness after different abrasion distances. The insets show the corresponding WCA and WSA.

In our previous studies, the Co-Ni coating and Co-Ni/WC composite coating were also prepared to investigate the mechanical durability by liner abrasion test[21,36]. The micro-hardness (HV), Roughness (*R*a) and abrasion distance values of these coatings were summarized in Table 2. We have found that some features were of vital importance for the wear resistance of super-hydrophobic coatings, such as the micro-nano hierarchical structures and micro-hardness. As indicated by the results, micro-hardness and roughness showed a positive correlation with the abrasion distance of the super-hydrophobic composite coatings. To improve the wear resistance of the super-hydrophobic coating, its microhardness was improved by adding second phase particles, which was proved effective through our works[21,36].

Table 2. The microhardness (HV), surface roughness (*Ra*) and abrasion distance values of the as-prepared coatings.

Coating	**Co-Ni coating**	**Co-Ni/WC composite coating**	**Co-Ni/CeO_2 composite coating**

Microhardness (HV)	217.8	334.4	305.1
Surface roughness (*Ra*, μm)	9.44	14.65	10.41
Abrasion distance (m)	12	34	22.5

The testing of qualitative surface energy on the super-hydrophobic coating includes self-cleaning effect (Fig.7). Fig.7a displayed the photograph of static water droplet on the super-hydrophobic Co-Ni/CeO_2 coating electrodeposited with 3.44 g/L CeO_2 particles contents and the measured WCA was over 160° (Fig.5a). The dynamic process of droplet impacting on the super-hydrophobic surface was recorded with a high speed camera. As shown in Fig.7b, 3-rebounds process for a 15 μL liquid drops with 1 cm release height was captured within one second before bouncing off the recording area, suggesting the rapid drop detachment and reduced liquid-solid contact time of water droplets on the as-prepared super-hydrophobic coating[37].

The self-cleaning effect is another significant property for super-hydrophobic coating. Through spreading Al_2O_3 powders deliberately on the super-hydrophobic surface with a slope angle of about 10° above the horizontal, the self-cleaning test was carried out. As shown in Fig.7c-7e, the self-cleaning behavior was demonstrated by easily rolling off in a short time and absorbing the powder immediately with the dropping of water droplet. The result could be attributed to the extremely low surface free energy after modification by PFTEOS [38]. Therefore, the powders could be easily removed by the water droplets during the rolling process, which revealed an excellent self-cleaning effect of the our super-hydrophobic Co-Ni/CeO_2 composite coating.

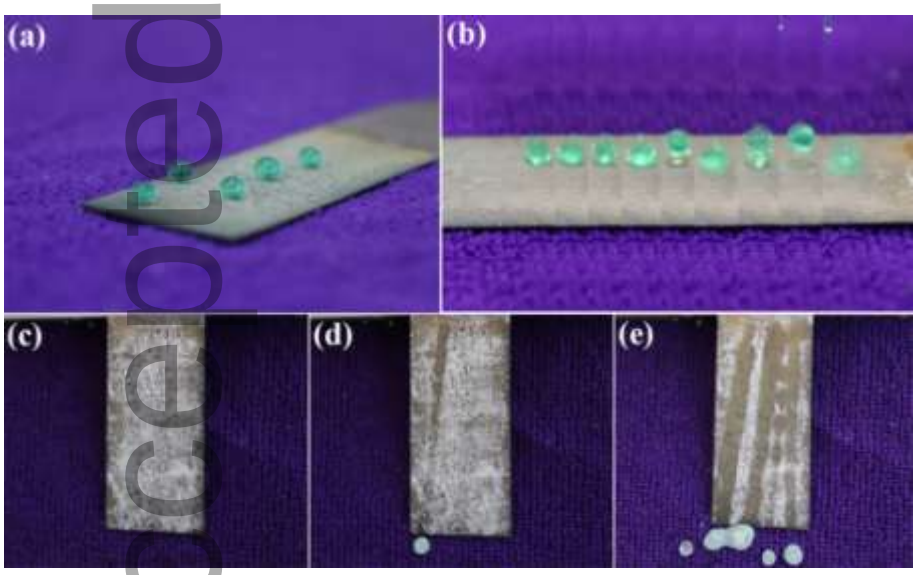

Figure 7. Demonstartion of super-hydrophobicity for as-prepared Co-Ni/CeO_2 coating electrodeposited with 3.44 g/L CeO_2 particles: (a) Water droplet staying on the coating; (b) An deionized water droplet bouncing; (c-e) The self-cleaning behavior.

The corrosion behaviors of the super-hydrophobic Co-Ni/CeO_2 coatings with high wear resistance and bare carbon steel substrate were assessed in a 3.5 wt.% NaCl solution (Fig.8). Compared to bare carbon steel, all the super-hydrophobic coatings have much higher corrosion potential values and lower corrosion current densities. For the super-hydrophobic Co-Ni/CeO_2 composite coating (1.72 g/L CeO_2 and 3.44 g/L CeO_2), the corrosion potentials shift positively about 109 mV and 142 mV,respectively. Due to the adding of CeO_2 particles, the corrosion probability of the as-prepared super-hydrophobic coatings decreases. However, with the increasing of micro-nano CeO_2 particles to

6.88 g/L, corrosion potential shift negatively a little, which could be attributed to the formation of holes based on the difficulty of co-electrodeposition under the deposition conditions of large amount of CeO_2 particles in the mixed solution.

As seen from Table 2, the as-prepared super-hydrophobic coatings electrodeposited with the CeO_2 particles of 1.72 g/L and 3.44 g/L exhibited a two orders of magnitude reduction in corrosion rate, which could be attributed to their super-hydrophobicity that the trapped air as a barrier decreased the solution/solid contact area effectively. For the super-hydrophobic coating electrodeposited with the 6.88 g/L CeO_2 particles, the corrosion current density (i_{corr}) was smaller than those of the aforementioned composite coatings. By the addition of the CeO_2 particles, the super-hydrophobic coating was denser, which thereby results in lower corrosion current density. These results indicated that the corrosion resistance of the super-hydrophobic coating depends on not only the surface wettability but also the coating density.

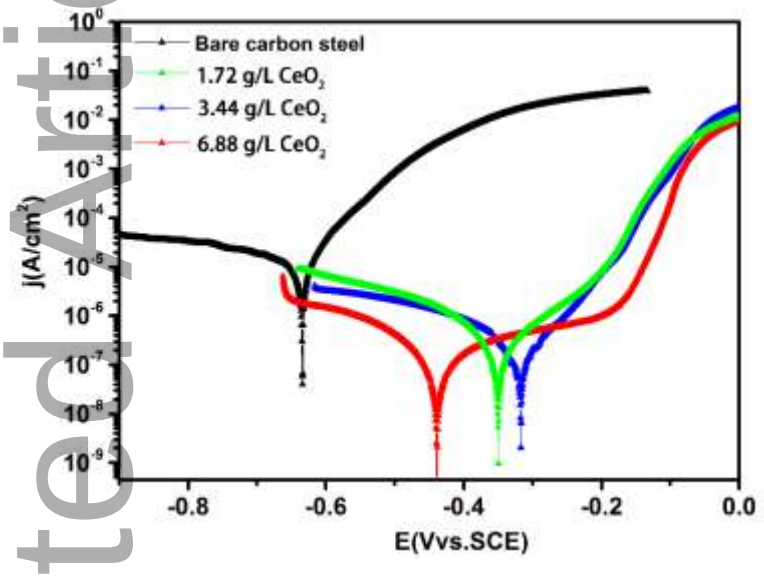

Figure 8. Potentiodynamic polarization curves of the bare carbon steel and the as-prepared super-hydrophobic coatings in 3.5 wt.% NaCl solution at sweep speed of 0.5 mV/s.

Table 3. The corrosion parameters estaimated through the Tafel extrapolation according to the polarization measurements.

Sample	E_{corr} (mV)	i_{corr} (A/cm^2)	Corrosion rate (μm/year)
Bare carbon steel	-459	1.23×10^{-5}	137.0
Super-hydrophobic coating (1.72g/L CeO_2)	-350	1.78×10^{-7}	1.91
Super-hydrophobic coating (3.44g/L CeO_2)	-317	1.24×10^{-7}	1.42
Super-hydrophobic coating (6.88g/L CeO_2)	-439	8.06×10^{-8}	0.90

The EIS results were shown in Fig. 9 for the super-hydrophobic Co-Ni/CeO_2 coatings and carbon steel substrate. The best fitting data with an appropriate equivalent circuit model were also included

in the plots as solid lines. Fig. 9a showed the existence of one unfinished capacitive loop with different sizes for each sample. Generally, the larger size of the capacitive loop represents greater corrosion resistance of a coating. In the Nyquist plots, a larger capacitive loop was clearly observed for the as-prepared super-hydrophobic Co-Ni/CeO_2 coatings electrodeposited with the 3.44 g/L CeO_2 particles. In the Bode plots of modular impedance against frequency (Fig. 9b), the modular impedance (Z) for the composite coatings displayed a liner slope in low and middle frequency range, with the maximum values of as large as about 350 $k\Omega \cdot cm^2$, which is 2 orders of magnitude higher than 1.75 $k\Omega \cdot cm^2$ for the bare carbon steel. In the Bode plots of phase angle against frequency (Fig. 9c), only one time constant was observed for the bare carbon steel, and the phase angle reached their maximum values in the region of intermediate frequencies, which was the characteristic response of a capacitive behavior. However, two distinct time constants were observed for the as-prepared Co-Ni/CeO_2 composite coatings, from which the high frequency time constant was related to the formation of super-hydrophobic/hydrophobic coatings and the intermediate frequency time constant could be ascribed to the capacitance of double layer.

To analysis the impedance data accurately, different equivalent circuit (EC) models were used for EIS experimental data analysis with ZSimpWin software, and the fitting results were displayed in Fig. 9d and 9e for the carbon steel substrate and the Co-Ni/CeO_2 composite coatings, respectively. The equivalent circuit model shown in Fig. 9d revealed the electrochemical behavior of bare carbon steel at the electrode/electrolyte interface. In this circuit, R_s corresponds to the solution resistance, CPE_{dl} and R_{ct} corresponds to the double layer capacitance and charge transfer resistance at the interface. The constant phase element (CPE) represents the possibility of a non-ideal capacitance due to the heterogeneities at the electrode surface. From literatures[39], the impedance of CPE (Z_{CPE}) is defined as below:

$$Z_{CPE} = 1/Y_0(j\omega)^n$$

Where Y_0 is the admittance, j is the imaginary number, ω is the angular frequency and n is an empirical exponent of the CPE[40]. Furthermore, the value of n varying between 0 and 1.

The equivalent circuit model shown in Fig. 9e revealed the corrosion process of Co-Ni/CeO_2 composite coatings which was classically used to speculate the non-ideal capacitive behavior of the passive film with porous structures. In this circuit, the CPE_c and R_c correspond to the double layer capacitance at the coating/solution interface and charge transfer resistance of the Co-Ni/CeO_2 composite coatings, respectively. In this case, the trapped airs among the hierarchical structures limited the contact area of Co-Ni/CeO_2 coating with the NaCl solution as well as the coatings hindered the corrosion process at the interface. And the R_{ct} and CPE_{dl} are related to the charge transfer resistance and double layer capacitance happening at the coating/substrate interface.

Based on the selected equivalent circuits, the fitting data is shown in Table 4, which clearly indicated an increasing tendency of R_c and R_{ct} for composite coatings. Compared to bare carbon steel, the values of R_{ct} were evidently more than one order of magnitude larger and the derived CPE_{dl} were much less for all three Co-Ni/CeO_2 composite coatings. In addition, the values of R_c were approximately close to 400 $k\Omega \cdot cm^2$ for all three Co-Ni/CeO_2 composite coatings. In particular, the decrease of CPE_{dl} and increase of R_{ct} suggested the gradual growth of protective for inner layer, which indicated the limiting of the charge transfer process. Decrease of CPE_c accompanying with increase of R_c suggested that the composite coating became thicker and more protective as the content increase of CeO_2[41]. Based on the higher value of R_c than R_{ct}, the main protection can be attributed to

the prepared super-hydrophobic Co-Ni/CeO_2 composite coatings.

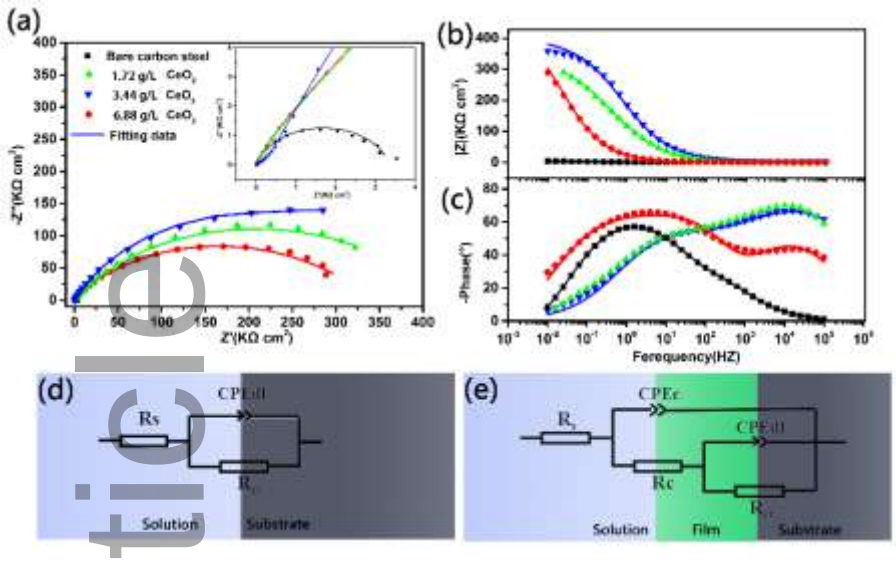

Figure 9. EIS results recorded in 3.5 wt.% NaCl solution: (a) Nyquist plots; (b) Modular impedance versus frequency plots and (c) Phase angle versus frequency plots. (d) Equivalent circuit for the carbon steel. (e) Equivalent circuit for Co-Ni/CeO_2 coatings.

Table 4. The EIS parameters estimated by fitting with the equivalent circuits.

Fitted parameters	R_s	CPE_{dl}	n_{dl}	R_{ct}	CPE_c	n_c	R_c
Bare carbon steel	8.32	1.08×10^{-3}	0.659	2.35	-	-	-
1.72 g/L CeO_2	13.31	2.84×10^{-7}	0.7762	102.1	9.74×10^{-7}	0.6275	391
3.44 g/L CeO_2	12.69	2.78×10^{-7}	0.7781	95.9	1.04×10^{-6}	0.5861	401
6.88 g/L CeO_2	12.74	6.43×10^{-6}	0.669	43.24	5.07×10^{-6}	0.7891	436

Note: The units of R_s, R_{ct}, R_c and CPE are $\Omega\cdot cm^2$, $k\Omega\cdot cm^2$, $k\Omega\cdot cm^2$ and $\Omega^{-1}\cdot s^n\cdot cm^{-2}$, respectively.

4. Conclusion

In summary, the Co-Ni/CeO_2 coatings containing hydrophobic CeO_2 particles were prepared by co-electrodepositon. And the Co-Ni/CeO_2 coating electrodeposited with the 3.44 g/L CeO_2 particles exhibited a flower-like micro/nano hierarchical structures with water contact angle of 160.7° after the PFTEOS modification. The linear abrasion test results revealed that the composite coating could maintain the critical abrasion distance of 22.5 m before the loss of super-hydrophobicity. And the rolling process tests of water droplets on the large-scale samples revealed an excellent self-cleaning effect of our super-hydrophobic coating. Furthermore, electrochemical measurements demonstrated that the corrosion rate of our prepared super-hydrophobic composite coatings showed 2 orders of magnitude drop than the carbon steel substrate due to their super-hydrophobicity that the trapped air prevented the permeation of corrosive electrolyte ions at the coating/solution interface. Nowadays, the long-term stability of our super-hydrophobic composite coating is being evaluated for the potential applications in the marine field.

Acknowledgement

Dr. Xue thanks the support from Fundamental Research Funds for the Central Universities China (Project ID: FRF-TP-18-009A1). And the project was also supported by the Tribology Science Fund of State Key Laboratory of Tribology.

Conflict of Interest

The authors declare no conflict of interest.

Keywords: Cerium oxide particles; Wettability; Electrodeposition; Wear resistance; Self-cleaning; Marine corrosion;

Reference

[1] E. Vazirinasab, R. Jafari, G. Momen, *Surf. Coatings Technol.* **2018**, *341*, 40.
[2] W. Tong, D. Xiong, H. Zhou, *Ceram. Int.* **2020**, *46*, 1211.
[3] M. Ge, C. Cao, J. Huang, X. Zhang, Y. Tang, X. Zhou, K. Zhang, Z. Chen, Y. Lai, *Nanoscale Horizons* **2018**, *3*, 235.
[4] S. Bano, U. Zulfiqar, U. Zaheer, M. Awais, I. Ahmad, T. Subhani, *Adv. Eng. Mater.* **2018**, *20*, 201700460.
[5] P. Eberle, M. K. Tiwari, T. Maitra, D. Poulikakos, *Nanoscale* **2014**, *6*, 4874.
[6] X. Yin, S. Yu, X. Bi, E. Liu, Y. Zhao, *Ceram. Int.* **2019**, *45*, 24618.
[7] G. He, S. Lu, W. Xu, T. Yu, J. Li, T. Dai, *Ceram. Int.* **2018**, *44*, 638.
[8] X. Pu, G. Li, H. Huang, *Biol. Open* **2016**, *5*, 389.
[9] K. Liu, L. Jiang, *Nanoscale* **2011**, *3*, 825.
[10] R. Liao, Z. Zuo, C. Guo, Y. Yuan, A. Zhuang, *Appl. Surf. Sci.* **2014**, *317*, 701.
[11] J. Yu, L. Qin, Y. Hao, S. Kuang, X. Bai, Y. Chong, W. Zhang, E. Wang, *ACS Nano* **2010**, *4*, 414.
[12] J. Long, P. Fan, D. Gong, D. Jiang, H. Zhang, L. Li, M. Zhong, *ACS Appl. Mater. Interfaces* **2015**, *7*, 9858.
[13] C. V. Ngo, D. M. Chun, *Adv. Eng. Mater.* **2018**, *20*, 1701086.
[14] M. Lee, G. Kwak, K. Yong, *ACS Appl. Mater. Interfaces* **2011**, *3*, 3350.
[15] J. Li, Y. Lu, Z. Wu, Y. Bao, R. Xiao, H. Yu, Y. Chen, *Ceram. Int.* **2016**, *42*, 9621.
[16] C. Jeong, C. H. Choi, *ACS Appl. Mater. Interfaces* **2012**, *4*, 842.
[17] D. Quéré, *Annu. Rev. Mater. Res.* **2008**, *38*, 71.
[18] A. Starostin, V. Valtsifer, V. Strelnikov, E. Bormashenko, R. Grynyov, Y. Bormashenko, A. Gladkikh, *Adv. Eng. Mater.* **2014**, *16*, 1127.
[19] Y. Xue, S. Wang, G. Zhao, A. Taleb, Y. Jin, *Surf. Coat. Technol.* **2019**, *363*, 352.
[20] T. Wang, J. Cai, Y. Wu, T. Hang, A. Hu, H. Ling, M. Li, *ACS Appl. Mater. Interfaces* **2019**, *11*, 11106.
[21] Y. Xue, S. Wang, P. Bi, G. Zhao, Y. Jin, *Coatings* **2019**, *9*, 232.
[22] J. He, J. He, M. Yuan, M. Xue, X. Ma, L. Hou, T. Zhang, X. Liu, M. Qu, *Adv. Eng. Mater.* **2018**, *20*, 1701180.
[23] T. Darmanin, E. T. De Givenchy, S. Amigoni, F. Guittard, *Adv. Mater.* **2013**, *25*, 1378.
[24] X. Yanpeng, A. Taleb, P. Jegou, *J. Mater. Chem. A* **2013**, *1*, 11580.
[25] Z. She, Q. Li, Z. Wang, L. Li, F. Chen, J. Zhou, *Chem. Eng. J.* **2013**, *228*, 415.
[26] J. Tam, Z. Jiao, J. C. F. Lau, U. Erb, *Wear* **2017**, *374–375*, 1.
[27] G. Zhao, Y. Xue, Y. Huang, Y. Ye, F. C. Walsh, J. Chen, S. Wang, *RSC Adv.* **2016**, *6*, 59104.
[28] J. Zhou, G. Zhao, J. Li, J. Chen, S. Zhang, J. Wang, F. C. Walsh, S. Wang, Y. Xue, *Appl. Surf. Sci.* **2019**, *487*, 1329.

[29] G. Azimi, R. Dhiman, H. M. Kwon, A. T. Paxson, K. K. Varanasi, *Nat. Mater.* **2013**, *12*, 315.
[30] J. Tam, G. Palumbo, U. Erb, G. Azimi, *Adv. Mater. Interfaces* **2017**, *4*, 1.
[31] *ASM Handbook: volume 3: Alloy Phase Diagrams*; 10th ed.; ASM International, 1992.
[32] N. Wang, T. Hang, S. Shanmugam, M. Li, *CrystEngComm* **2014**, *16*, 6937.
[33] D. Chandler, *Nature* **2005**, *437*, 640.
[34] N. Giovambattista, P. G. Debenedetti, P. J. Rossky, *Proc. Natl. Acad. Sci. U. S. A.* **2009**, *106*, 15181.
[35] X. Tian, T. Verho, R. H. A. Ras, *Science (80-.).* **2016**, *352*, 142.
[36] S. Wang, Y. Xue, C. Ban, Y. Xue, A. Taleb, Y. Jin, *Surf. Coat. Technol.* **2020**, *385*, 125390.
[37] J. Song, M. Gao, C. Zhao, Y. Lu, L. Huang, X. Liu, *ACS Nano* **2017**, *11*, 9259.
[38] W. Li, Z. Kang, *Surf. Coatings Technol.* **2014**, *253*, 205.
[39] P. Wang, T. Li, D. Zhang, *Corros. Sci.* **2017**, *128*, 110.
[40] M. Nie, C. T. Wang, M. Qu, N. Gao, J. A. Wharton, T. G. Langdon, *J. Mater. Sci.* **2014**, *49*, 2824.
[41] Z. Cui, L. Wang, H. Ni, W. Hao, C. Man, S. Chen, X. Wang, Z. Liu, X. Li, *Corros. Sci.* **2017**, *118*, 31.

The Co-Ni/CeO_2 composite coating with the hierarchical micro-nano structures fabricated by electrochemical deposition displays super-hydrophobic properties. The linear abrasion test indicates that the prepared super-hydrophobic Co-Ni/CeO_2 composite coating displays excellent mechanical durability with super-hydrophobicity for abrasion distance of 22.5 m. Furthermore, the super-hydrophobic Co-Ni/CeO_2 coating can provide better corrosion protection for the carbon steel substrate.